Dynamics of Space-Charge Domains in Ultrapure Ge

A. M. Kahn,[a] D. J. Mar, and R. M. Westervelt

Division of Applied Sciences and Department of Physics, Harvard University, Cambridge, Massachusetts 02138

(Received 3 September 1991)

An array of capacitive probes is used to measure the spatially dependent electric field associated with a driven chaotic instability in p-type ultrapure Ge. As the drive amplitude is increased, we observe first the onset of temporal chaos and later a transition to a higher-dimensional attractor with a loss of spatial coherence due to the nucleation and destruction of high-field domains in the bulk of the sample.

PACS numbers: 72.20.Ht, 47.20.Tg, 85.30.Fg

The role of spatial degrees of freedom in temporally chaotic systems is currently of great interest and has been experimentally explored in one-dimensional fluid [1-3] and chemical [4] systems. Recently, Mosekilde *et al.* reported spatiotemporal chaos in numerical simulations of a semiconductor system, driven Gunn diodes [5]. Held and Jeffries investigated the spatial structure of a helical instability [6,7] in an electron-hole plasma in n-type Ge at 77 K. Spontaneous current instabilities due to impurity impact ionization have been observed at low temperatures ($T < 30$ K) in Ge [8-11], GaAs [12], InSb [13], and Si [14]. Semiconductor instabilities are of interest because the dynamics of space charge in semiconductors can play an important role in photoconductors and high speed devices. These instabilities are well suited for experimental studies of nonlinear dynamics due to their accessible time scales and excellent dynamic range.

A spontaneous periodic current oscillation is observed in voltage-biased p-type ultrapure Ge at liquid-helium temperatures [9]. Using a movable capacitive probe, Kahn, Mar, and Westervelt [15] found that each period of the oscillation is associated with the nucleation and motion of a single high-field domain along the conduction direction. Gwinn and Westervelt [11,16] used this system to verify to high precision the universality of temporal behavior at the quasiperiodic transition to chaos. They showed that the dynamics are well described by a low-dimensional circle map model at the critical line, even though this is a spatially extended system. In this Letter we use an array of capacitive probes to investigate the spatially dependent electric field associated with driven chaotic oscillations. For drive amplitudes just above the critical line, the chaotic oscillation is low dimensional, in agreement with the results of Gwinn and Westervelt [11,16], and a single domain is observed traversing the sample. When the oscillation is driven chaotic well above the critical line, we observe a transition to a higher-dimensional attractor and a gradual loss of spatial coherence due to the nucleation and destruction of domains in the bulk of the sample. A similar loss of spatial coherence was observed for a helical instability in Ge [6]. In our experiment the voltage bias provides a feedback mechanism by which the different parts of the sample interact, since at all times the integrated electric field is fixed by the overall bias.

The samples were grown at Lawrence Berkeley Laboratory and were cut from the same crystal as those used previously by Gwinn and Westervelt [11,16] and by Kahn, Mar, and Westervelt [15]. The crystal is p-type ultrapure Ge with a shallow acceptor concentration $\sim 1 \times 10^{11}$ cm^{-3}, with characteristics described in Ref. [15]. Ohmic p^+ contacts are fabricated using B-ion implantation to degenerately dope a thin layer of germanium. The samples are rectangular with dimensions $14.5 \times 4.0 \times 4.0$ mm^3 and contacts across both 4×4 mm^2 faces. We chose this geometry so that electric-field lines lie along the length of the samples and variations in the electric field occur primarily along the conduction direction. We have experimentally verified the absence of current filaments in similar samples prepared with the same method [17].

The behavior of this system under dc voltage bias has been explored previously [15]. At a well-defined threshold in the applied electric field [voltage/(sample length)] $E_{\mathrm{dc}} = 3.2$ V/cm, the sample current increases by several orders of magnitude due to impact ionization of shallow acceptors. When E_{dc} is increased to $E_c = 6.30$ V/cm the onset of periodic current oscillations is observed. Each oscillation period is due to a single high-field domain composed of trapped charge which periodically traverses the sample [15]. For all results reported here the dc part of the applied electric field is fixed at $E_{\mathrm{dc}} = 7.45$ V/cm, which is above the threshold field E_c for spontaneous periodic current oscillations. The fundamental frequency f_0 of the spontaneous oscillation for this dc bias is 1.20 kHz. Several theoretical models [18-20] predict a region of N-shaped negative differential resistivity (NDR) in the plot of local current density versus local electric field in the postbreakdown regime. It is well known that voltage-biased samples with such an N-shaped characteristic may be unstable to the formation of moving high-electric-field domains, resulting in current oscillations [21].

In order to measure the spatially dependent electric field associated with nonperiodic current oscillations, an array of sixteen capacitive probes is fabricated on a sapphire substrate using photolithography. The probes are arranged in eight equal pairs as illustrated in Fig. 1. The sample is laid on top of the array with the probes oriented

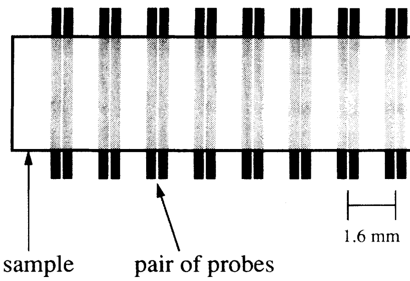

FIG. 1. Top view of the experimental geometry, showing array of paired capacitive probes. Each probe is 300 μm wide. Within each pair the center-to-center distance between probes is 400 μm.

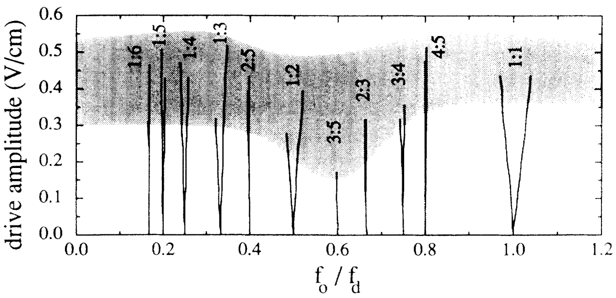

FIG. 2. Arnold-tongue diagram showing low-order lockings as a function of f_0/f_d and drive amplitude A. The shading is drawn to indicate the location of the critical line.

perpendicular to the conduction direction. Each probe is 300 μm wide, extends across the sample, and couples to it with a capacitance ≈ 0.2 pF. The current induced in each probe by the local time-dependent sample voltage is integrated and amplified using a charge-coupled amplifier [15]. There is negligible cross talk between probes because each probe is at virtual ground. The amplifier outputs are simultaneously digitized using a sixteen-channel transient recorder operated at 50 kHz, and the recorded voltages are normalized with respect to variations in capacitance between the probes. The local electric field $E(x,t)$ is determined at eight positions along the sample by taking the difference between sample voltages within each pair. The spatial resolution for measuring $E(x,t)$ is approximately 400 μm, the center-to-center distance between probes. The sample temperature is maintained at 4.2 K by immersion in liquid helium maintained at 1 atm. A sinusoidal ac drive voltage is superimposed upon the dc bias voltage, so that the total applied electric field is given by $E_{\mathrm{total}}(t) = E_{\mathrm{dc}} + A\sin(2\pi f_d t)$, where E_{dc} is the dc part of the applied field, A is the drive amplitude, and f_d is the drive frequency. The sample current is measured by amplifying the voltage across a small (10 Ω) series resistor.

The frequency-locking behavior of the driven oscillation is described by the set of Arnold tongues shown in Fig. 2, with the drive amplitude A along the vertical axis and the frequency ratio f_0/f_d along the horizontal axis. Application of the drive may shift the fundamental frequency from f_0 to f_s, and the oscillation may lock onto the drive over a range of frequencies. The locking ratio f_s/f_d is indicated above each tongue. Experimentally, each tongue is mapped by varying the frequency and amplitude of the applied drive and determining when the oscillation becomes unlocked using a spectrum analyzer. In Fig. 2 the tongues extend for increasing drive amplitude until hysteresis is first observed in the boundary of the tongue. It has been shown [11,16] that this system is well described at the quasiperiodic transition to chaos by the circle map. In this model, hysteresis occurs only above the critical line where the map becomes noninvertible. The tops of the Arnold tongues in Fig. 2 approximate the critical line, which need not be smooth; above the critical line it is possible to drive the oscillation chaotic.

Figure 3 shows Poincaré maps of the sample current driven in the chaotic regime for two different sets of drive parameters. These plots are constructed by sampling the current $I_n(\varphi)$ at a fixed drive phase φ and plotting the first return map I_{n+1} vs I_n. The drive amplitude used for Fig. 3(a) is $A=0.85$ V/cm, above the critical line in Fig. 2, and the drive frequency is at $f_0/f_d=0.62$, approximately equal to the golden mean $\sigma_g=(\sqrt{5}-1)/2$. The folds in the Poincaré map at the bottom and along the right in Fig. 3(a) are characteristic of the wrinkled torus for the quasiperiodic transition to low-dimensional chaos. Figure 3(b) shows the Poincaré map resulting from a drive with larger amplitude and higher frequency, with $A=1.91$ V/cm and $f_0/f_d=0.18$. The sample current is again chaotic but in this case the Poincaré map has a much fuzzier appearance, indicative of a higher-dimensional attractor.

Figure 4(a) shows the measured spatial structure associated with the driven chaotic oscillation over a number of oscillation periods, using the same drive parameters as for Fig. 3(a). The local time-dependent electric field is shown at eight equally spaced positions along the sample; the trace taken closest to the injecting contact is at the bottom of Fig. 4(a). The figure clearly shows that the time dependence of the oscillation is due to a single domain traversing the sample. Thus, even though the

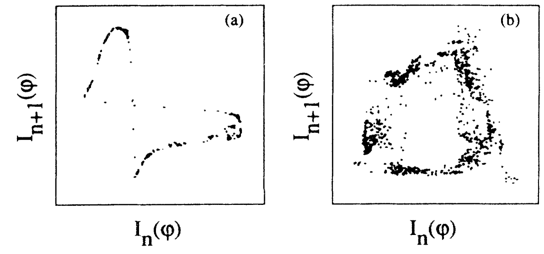

FIG. 3. Poincaré map of the sample current for (a) drive amplitude $A=0.85$ V/cm and $f_0/f_d=0.62$; (b) $A=1.91$ V/cm and $f_0/f_d=0.18$.

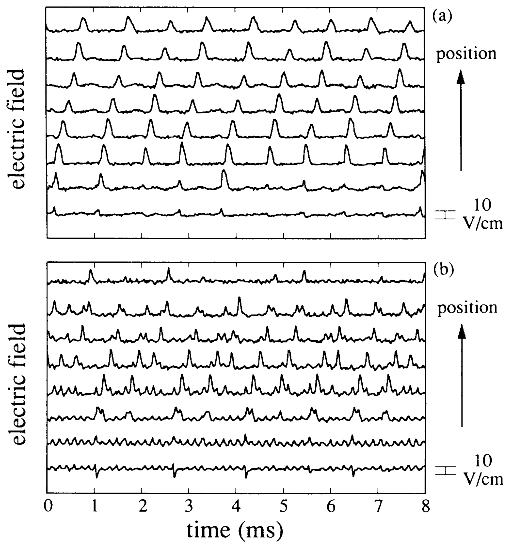

FIG. 4. Local sample electric field vs time at successive positions along the sample for (a) drive amplitude $A = 0.85$ V/cm and $f_0/f_d = 0.62$, as used for Fig. 3(a); (b) $A = 1.91$ V/cm and $f_0/f_d = 0.18$, as used for Fig. 3(b). The bottom trace is taken closest to the injecting contact in both figures.

current is temporally chaotic, the electric-field variations are spatially coherent. High-field domains are nucleated only near the injecting contact. Each domain moves smoothly through the sample and always reaches the receiving contact. A new domain is nucleated only as the previous domain leaves through the receiving contact. The nonperiodic nature of the oscillation is manifested as a variation in the amplitude of the domains when they first enter the sample and as a variation in the intervals between domains.

Figure 4(b) shows electric-field traces $E(x,t)$ associated with the driven chaotic oscillation using the same parameters as for the Poincaré map in Fig. 3(b). The spatial structure shown in Fig. 4(b) is much more complicated than that in Fig. 4(a). In particular, Fig. 4(b) shows individual domains being nucleated and destroyed in the bulk of the sample, and at times there are multiple domains in the sample. The bottom two traces in Fig. 4(b) show fluctuations in $E(x,t)$ at the drive frequency. The next several traces show the growth and decay of larger structures. Very few of the domains in Fig. 4(b) succeed in reaching the last pair of capacitive probes, which is 1.6 mm from the receiving contact. The complex spatial structure shown in Fig. 4(b) shows that for this set of drive parameters many degrees of freedom are important, as suggested by the Poincaré map in Fig. 3(b).

We have measured the effect of the ac drive on spatial coherence over a range of drive parameters. As a measure of the spatial coherence, we use the linear correlation coefficient $r_t(x,\tau)$ defined as [22]

$$r_t(x,\tau) = \frac{\sum_d E(d,t)E(d-x,t+\tau)}{[\sum_d E(d,t)^2 \sum_d E(d-x,t+\tau)^2]^{1/2}}, \qquad (1)$$

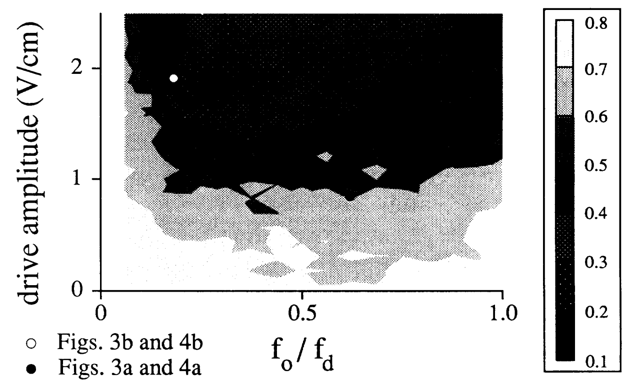

FIG. 5. Density plot of the maximum value of the linear correlation coefficient $r(x = 1.6\text{ mm}, \tau)$, as a function of f_0/f_d and drive amplitude A. The black dot ($A = 0.85$ V/cm, $f_0/f_d = 0.62$) indicates the parameters used for Figs. 3(a) and 4(a) and the white dot ($A = 1.91$ V/cm, $f_0/f_d = 0.18$) indicates the parameters used for Figs. 3(b) and 4(b).

where x and d are discrete distances along the conduction direction and τ is a time interval measured from an initial time t. This function is sensitive only to changes in the shape of the electric-field profile because the normalization in the denominator removes the effects of differences in the overall amplitudes of the signals. For each set of drive parameters we record $E(x,t)$ for 40 ms, and then calculate $r_t(x,\tau)$ using 1000 different values of t, separated by 40 μs. We then average over t to determine $r(x,\tau) = \langle r_t(x,\tau) \rangle_t$.

The shape of $r(x,\tau)$ vs τ is peaked at the time for a domain to move a distance x. For the example of the spatially coherent oscillation shown in Fig. 4(a) ($A = 0.85$ V/cm and $f_0/f_d = 0.62$), the peak value and width are $r_{\max} \approx 0.7$ and $\Delta\tau \sim 0.2$ ms; for the spatially incoherent oscillation in Fig. 4(b) ($A = 1.91$ V/cm and $f_0/f_d = 0.18$), $r_{\max} \approx 0.4$ and $\Delta\tau \sim 0.2$ ms. Figure 5 plots $r_{\max}$ versus drive amplitude A and f_0/f_d for the spacing $x = 1.6$ mm between pairs of capacitive probes; note that the vertical axis extends further above the critical line than for Fig. 2. Figure 5 is constructed using twenty equally spaced drive amplitudes and sixteen drive frequencies equally spaced in f_0/f_d. The lighter regions in Fig. 5 correspond to drive parameters for which the domain motion is spatially coherent and the darker regions correspond to less correlated behavior. As shown the loss of spatial coherence occurs gradually; we do not find evidence of a sharp transition. The drive parameters used for Figs. 3 and 4 are indicated by dots in Fig. 5. As expected, the drive parameters used for Figs. 3(b) and 4(b) lie in a much darker (less correlated) region of Fig. 5 than do the parameters for Figs. 3(a) and 4(a).

The least correlated region at the upper left of Fig. 5 corresponds to drive parameters $A \approx 2$ V/cm and $f_0/f_d \approx 0.3$. This region of minimum correlation occurs when the drive period is comparable to a characteristic time $\Delta t \approx 0.3$ ms which is given by the domain velocity divided by the domain width. When A is sufficiently large ($A > 1.15$ V/cm), domains are created and destroyed in the bulk of the sample, as shown in Fig. 4(b). The formation of a domain inside the sample depends on the local profiles of electric field and trapped charge density. Different parts of the sample are coupled by the requirement that the spatial integral of the electric field equal the applied voltage. Approximating the local field by its average across the sample, formation and destruction of domains are expected to occur when the applied electric field is comparable to the instability threshold E_c. We observe that for very large drive amplitudes, domains are destroyed before they reach the receiving contact, and the peak value of the correlation coefficient increases.

The range of drive parameters shown in Fig. 5 includes regions in which the oscillation is frequency locked to the drive as well as regions of chaotic oscillations. The spatial coherence of the electric field for the driven oscillation is not strongly dependent on whether the oscillation is locked. The question of whether the oscillation is locked or chaotic can only be answered by examining a time series over a number of domain transit times. In contrast, the spatial coherence is determined by the behavior on a time scale which is a fraction of a transit time.

We thank L. L. Bonilla, F. J. Higuera, S. H. Strogatz, and S. W. Teitsworth for valuable discussions. One of us (D.J.M.) acknowledges support from AT&T Bell Laboratories. This work was supported in part by the U.S. Office of Naval Research under Grant No. N00014-89-J-1592.

---

[a] Current address: Department of Physics, University of California, Santa Barbara, CA 93106.

[1] M. Rabaud, S. Michalland, and Y. Couder, Phys. Rev. Lett. **64**, 184 (1990).

[2] I. Mutabazi, J. J. Hegseth, C. D. Andereck, and J. E. Wesfreid, Phys. Rev. Lett. **64**, 1729 (1990).

[3] P. Kolodner, J. A. Glazier, and H. Williams, Phys. Rev. Lett. **65**, 1579 (1990).

[4] W. Y. Tam, J. A. Vastano, H. L. Swinney, and W. Horsthemke, Phys. Rev. Lett. **61**, 2163 (1988).

[5] E. Mosekilde, R. Feldberg, C. Knudsen, and M. Hindsholm, Phys. Rev. B **41**, 2298 (1990).

[6] G. A. Held and C. Jeffries, Phys. Rev. Lett. **55**, 887 (1985).

[7] G. A. Held and C. Jeffries, Phys. Rev. Lett. **56**, 1183 (1986).

[8] B. K. Ridley and R. G. Pratt, J. Phys. Chem. Solids **26**, 21 (1965).

[9] S. W. Teitsworth, R. M. Westervelt, and E. E. Haller, Phys. Rev. Lett. **51**, 825 (1983).

[10] J. Peinke, A. Mühlbach, R. P. Huebener, and J. Parisi, Phys. Lett. **108A**, 407 (1985).

[11] E. G. Gwinn and R. M. Westervelt, Phys. Rev. Lett. **57**, 1060 (1986); **59**, 247(E) (1987).

[12] K. Aoki and K. Yamamoto, Phys. Lett. **98A**, 72 (1983).

[13] D. G. Seiler, C. L. Littler, R. J. Justice, and P. W. Milonni, Phys. Lett. **108A**, 462 (1985).

[14] K. Yamada, N. Takara, H. Imada, N. Miura, and C. Hamaguchi, Solid State Electron. **31**, 809 (1988).

[15] A. M. Kahn, D. J. Mar, and R. M. Westervelt, Phys. Rev. B **43**, 9740 (1991).

[16] E. G. Gwinn and R. M. Westervelt, Phys. Rev. Lett. **59**, 157 (1987).

[17] A. M. Kahn, D. J. Mar, and R. M. Westervelt, Solid State Electron. **32**, 1143 (1989).

[18] S. W. Teitsworth, Appl. Phys. A **48**, 127 (1989).

[19] L. L. Bonilla and S. W. Teitsworth, Physica (Amsterdam) **50D**, 545 (1991).

[20] V. V. Mitin, Appl. Phys. **39**, 123 (1986).

[21] B. K. Ridley, Proc. Phys. Soc. London **82**, 954 (1963).

[22] W. H. Press, B. P. Flannery, S. A. Teukolsky, and W. T. Vetterling, *Numerical Recipes* (Cambridge Univ. Press, New York, 1986).

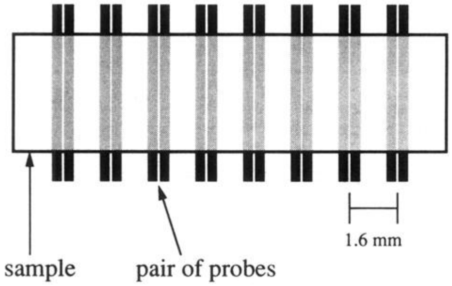

FIG. 1. Top view of the experimental geometry, showing array of paired capacitive probes. Each probe is 300 μm wide. Within each pair the center-to-center distance between probes is 400 μm.

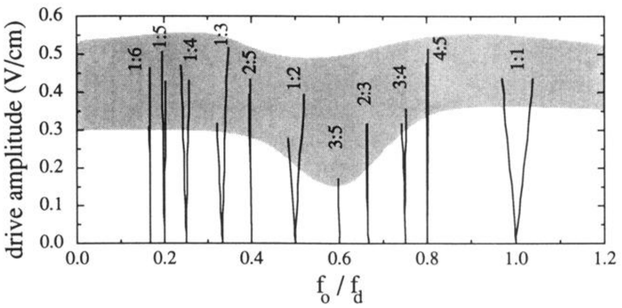

FIG. 2. Arnold-tongue diagram showing low-order lockings as a function of f_0/f_d and drive amplitude A. The shading is drawn to indicate the location of the critical line.

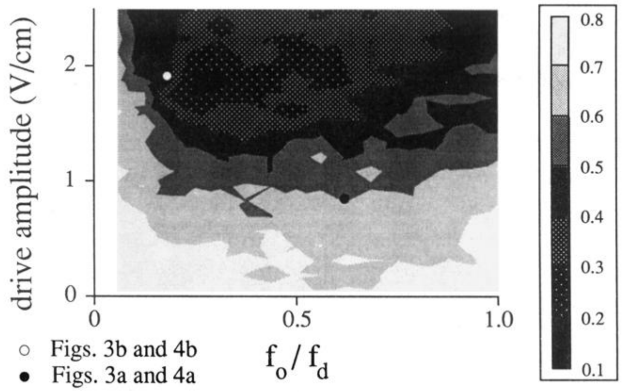

FIG. 5. Density plot of the maximum value of the linear correlation coefficient $r(x=1.6\ \text{mm},\ \tau)$, as a function of f_0/f_d and drive amplitude A. The black dot ($A=0.85$ V/cm, $f_0/f_d=0.62$) indicates the parameters used for Figs. 3(a) and 4(a) and the white dot ($A=1.91$ V/cm, $f_0/f_d=0.18$) indicates the parameters used for Figs. 3(b) and 4(b).